Z_3 symmetric inert $(2+1)$-Higgs-doublet model

A. Aranda,[1,*] D. Hernández-Otero,[2,†] J. Hernández-Sanchez,[3,‡] V. Keus,[4,5,§] S. Moretti,[5,‖] D. Rojas-Ciofalo,[5,¶] and T. Shindou[6,**]

[1]*Facultad de Ciencias-CUICBAS, Universidad de Colima, Bernal Díaz del Castillo 340, Colima 28045, Mexico*
[2]*Instituto de Física, Benemérita Universidad Autónoma de Puebla, Apartado Postal J-48, C.P. 72570 Puebla, Puebla, Mexico*
[3]*Facultad de Ciencias de la Electrónica, Benemérita Universidad Autónoma de Puebla, Apartado Postal 542, C.P. 72570 Puebla, Puebla, Mexico*
[4]*Department of Physics and Helsinki Institute of Physics, University of Helsinki, Gustaf Hallstromin katu 2, Helsinki FIN-00014 Finland*
[5]*School of Physics and Astronomy, University of Southampton, Southampton SO17 1BJ, United Kingdom*
[6]*Division of Liberal-Arts, Kogakuin University, 2665-1 Nakano-machi, Hachioji, Tokyo 192-0015, Japan*

(Received 12 September 2020; accepted 26 December 2020; published 20 January 2021)

We introduce a three-Higgs doublet model (3HDM) with two inert (or dark) scalar doublets and an active Higgs one, hence termed I$(2+1)$HDM, in the presence of a discrete Z_3 symmetry acting upon the three doublet fields. We show that such a construct yields a dark matter (DM) sector with two mass-degenerate states of opposite *CP* quantum number, both of which contribute to DM dynamics, which we call "hermaphrodite DM," distinguishable from a (single) complex DM candidate. We show that the relic density contributions of both states are equal, saturating the observed relic density compliant with (in)direct searches for DM as well as other experimental data impinging on both the dark and Higgs sectors of the model, chiefly, in the form of electroweak precision observables, Standard Model-like Higgs boson measurements at the Large Hadron Collider and void searches for additional (pseudo)scalar states at the CERN machine and previous colliders.

DOI: 10.1103/PhysRevD.103.015023

I. INTRODUCTION

The discovery of a Higgs boson by the Large Hadron Collider (LHC) in July 2012 [1,2] has finally confirmed that electroweak symmetry breaking (EWSB) is triggered by the Higgs mechanism. While such a new state of nature is perfectly consistent with the Standard Model (SM), which incorporates one Higgs doublet, there is no compelling reason to assume that there should be only one. In fact, it is possible that additional Higgs doublets exist such that their corresponding Higgs bosons could be found during one of the upcoming LHC runs. If one assumes that doublet (complex) representations of Higgs fields are those chosen by nature to implement EWSB, which is entirely plausible in the light of the fact that only such a structure is able to give mass to the $W^{\pm}$ and Z bosons of the SM while preserving a massless photon, thereby in turn enabling unification of electromagnetic (EM) and weak interactions, then one may wonder what can models with a generic number N of Higgs doublets, in turn defining the class of N-Higgs doublet models (NHDMs), produce in terms of new physics signals. The question is particularly intriguing if one further connects it to the need to explain the existence of dark matter (DM) in nature, something that is absent in the SM.

In order to attempt answering such a more articulate question, one may concentrate on the class of two-Higgs doublet models (2HDMs) [3]. In doing so, one should make sure to realize a 2HDM in a structure within which the DM candidate is a *stable* (on cosmological time scales), *cold* (i.e., nonrelativistic) at the onset of galaxy formation, *nonbaryonic*, *neutral* and *weakly interacting* component of the Universe [4]. A very simple 2HDM realization that provides a scalar DM candidate is the model with one inert

*fefo@ucol.mx
†danielah@ifuap.buap.mx
‡jaime.hernandez@correo.buap.mx
§venus.keus@helsinki.fi
‖S.Moretti@soton.ac.uk
¶D.Rojas-Ciofalo@soton.ac.uk
**shindou@cc.kogakuin.ac.jp

(I) doublet plus one Higgs (H) doublet, that we label as I$(1+1)$HDM. This 2HDM representation is known in the literature as the inert doublet model (IDM), which was proposed in 1978 [5] and has been studied extensively over many decades. In this scenario, one $SU(2)_L$ doublet with the same SM quantum numbers as the SM Higgs one is introduced. Here, a Z_2 symmetry is also introduced, under which the even parity is assigned to the SM Higgs doublet and the odd parity is assigned to the additional one. A possible vacuum configuration of this model is $(v,0)$, where the second doublet does not develop a vacuum expectation value (VEV) while the first one inherits the SM VEV, v.[1] With this vacuum configuration, the Z_2 symmetry remains unbroken after EWSB. In fact, the former does not take part in EWSB while the latter contains essentially the aforementioned Higgs state discovered at the CERN machine. Since the inert doublet does not couple to fermions, as it is by construction the only Z_2-odd field in the model, it provides a stable DM candidate. In essence, this is the lightest state among the two neutral (scalar and pseudoscalar) inert states with Z_2-odd quantum numbers (while all the SM states are Z_2 even).[2]

The next class of NHDMs is constituted by three-Higgs doublet models (3HDMs). The case for these is particularly promising for two main reasons. To begin with, 3HDMs are more tractable than higher multiplicity NHDMs as all possible finite symmetries have been identified [6,7]. Furthermore, and perhaps most intriguingly, 3HDMs may shed light on the flavor problem, namely the problem of the origin and nature of the three families of quarks and leptons, including neutrinos, and their pattern of masses, mixings and CP violation. Indeed, it is possible that the three families of SM fermions could be described by the same symmetries that describe the three Higgs doublets [8]. In such models this family symmetry could be spontaneously broken along with the EW one, with some remnant subgroup surviving, so that, for certain symmetries, it is possible to find a VEV alignment that respects the original symmetry of the scalar potential which will then be responsible for the stabilization of the DM candidate [9].

One could then simply extend the I$(1+1)$HDM by introducing another *inert* $SU(2)_L$ doublet with, again, the same SM quantum numbers as the SM Higgs one, thereby realizing a I$(2+1)$HDM, hence achieving the vacuum alignment $(0,0,v)$, which is of particular interest because of its similarity with the I$(1+1)$HDM and the absence of flavor changing neutral currents (FCNCs).[3]

The I$(2+1)$HDM has the following advantages over the I$(1+1)$HDM. First, the low and medium mass regions for the DM candidate ($m_{\rm DM} \lesssim 100$ GeV) which are excluded in the I$(1+1)$HDM are revived in the I$(2+1)$HDM due to the presence of more coannihilation channels [11]. Second, the extended dark sector in the I$(2+1)$HDM allows for the possibility of *dark CP violation*, a novel phenomenon first introduced in [12], which further revives the low DM mass region in comparison to the I$(1+1)$HDM. Note that, in order to introduce dark CP violation, it is necessary to at least add a singlet scalar to the I$(1+1)$HDM. However, the CP violating effects are smaller and less accessible to measure in the I$(1+1)$HDM plus a singlet compared to the I$(2+1)$HDM [13]. Third, in order to impose a Z_N symmetry with $N>2$ on the dark sector, again, at least one singlet should be added to the I$(1+1)$HDM. However, in this paper, we will probe Z_3 symmetric I$(2+1)$HDM solutions that satisfy several constraints for the low DM mass region which are instead excluded in the Z_3 symmetric I$(1+1)$HDM plus singlet. This Z_3 symmetric I$(2+1)$HDM is the model we will be concerned with, building upon the one introduced and studied in Refs. [14–19]. Herein, though, the discrete symmetry structure used was again a Z_2 one, like in 2HDMs, separating the two inert doublets and the active one. Again, the lightest Z_2-odd neutral scalar of this construct is the DM candidate.

In this paper, we study a variation of such a I$(2+1)$HDM, wherein we replace this Z_2 symmetry with a Z_3 one instead, following the example adopted in [20] for the case of a 2HDM. The motivation for this is to attempt generating a 3HDM with two mass-degenerate DM states with opposite CP. We shall in fact show that, in the case of a Z_3 symmetric scalar potential, such a DM setup, which we call "hermaphrodite DM," is indeed possible and distinguishable from a complex DM setup.

The layout of the remainder of the paper is as follows. In the next section we describe the aforementioned variation of the I$(2+1)$HDM with a Z_3 symmetry. In the following sections we discuss both theoretical and experimental constraints affecting our model. Numerical results and the selection of our benchmark scenarios will then follow while in the last section we will conclude.

II. THE I$(2+1)$HDM SCALAR POTENTIAL

In an NHDM, the generic scalar potential symmetric under a group G of phase rotations can be written as the sum of two parts:

[1]The doublet that acquires a VEV is called the *active* doublet and the one with no VEV is called the *inert* (at times also *dark*) doublet.

[2]Incidentally, notice that scalar (H) and pseudoscalar (A) particles from the inert doublet in the I$(1+1)$HDM have opposite CP quantum numbers but, as they do not couple to fermions, the only means of disentangling them is to exploit their gauge interactions: e.g., the HAZ vertex is present while the HHZ and AAZ ones are not.

[3]A 3HDM with $(0,v,v')$ vacuum alignment has been considered in [10] wherein it was termed IDM2. Using our nomenclature, this model may be referred to as the I$(1+2)$HDM.

$$V = V_0 + V_G, \tag{1}$$

where V_0 is invariant under any phase rotation and V_G is a collection of extra terms ensuring the symmetry under the action of the group G [21].

The most general phase invariant part of a 3HDM potential has the following form:

$$\begin{aligned} V_0 = & -\mu_1^2(\phi_1^\dagger\phi_1) - \mu_2^2(\phi_2^\dagger\phi_2) - \mu_3^2(\phi_3^\dagger\phi_3) \\ & + \lambda_{11}(\phi_1^\dagger\phi_1)^2 + \lambda_{22}(\phi_2^\dagger\phi_2)^2 + \lambda_{33}(\phi_3^\dagger\phi_3)^2 \\ & + \lambda_{12}(\phi_1^\dagger\phi_1)(\phi_2^\dagger\phi_2) + \lambda_{23}(\phi_2^\dagger\phi_2)(\phi_3^\dagger\phi_3) \\ & + \lambda_{31}(\phi_3^\dagger\phi_3)(\phi_1^\dagger\phi_1) + \lambda'_{12}(\phi_1^\dagger\phi_2)(\phi_2^\dagger\phi_1) \\ & + \lambda'_{23}(\phi_2^\dagger\phi_3)(\phi_3^\dagger\phi_2) + \lambda'_{31}(\phi_3^\dagger\phi_1)(\phi_1^\dagger\phi_3), \end{aligned} \tag{2}$$

where the notation of [11] was used. The construction of the Z_3 symmetric part of the potential depends on the generator of the Z_3 symmetry. As we want to study the model with two different DM candidates, in order to accomplish this, we will assign different charges to each doublet. More specifically, we assume that the Lagrangian is symmetric under the Z_3 transformation given by

$$\phi_1 \to \omega\phi_1, \qquad \phi_2 \to \omega^2\phi_2, \qquad \phi_3 \to \phi_3, \tag{3}$$

with ω being a complex cubic root of unity, $\omega = e^{2\pi i/3}$. In other words, we can write the generator of the group as follows:

$$g_{Z_3} = \mathrm{diag}(\omega, \omega^2, 1). \tag{4}$$

With these assignments, the Z_3 symmetric potential term V_G has the following form:

$$\begin{aligned} V_{Z_3} = & \lambda_1(\phi_2^\dagger\phi_1)(\phi_3^\dagger\phi_1) + \lambda_2(\phi_1^\dagger\phi_2)(\phi_3^\dagger\phi_2) \\ & + \lambda_3(\phi_1^\dagger\phi_3)(\phi_2^\dagger\phi_3) + \mathrm{H.c.} \end{aligned} \tag{5}$$

We take all the parameters of the potential to be real. We will identify ϕ_3 with the SM Higgs doublet and the Z_3 charges for all other SM particles are considered to be zero. The Yukawa Lagrangian in this model is identical to the SM Yukawa Lagrangian (with additional terms for right-handed neutrinos) given by

$$\begin{aligned} \mathcal{L}_Y = & \Gamma^u_{mn}\bar{q}_{m,L}\tilde{\phi}_3 u_{n,R} + \Gamma^d_{mn}\bar{q}_{m,L}\phi_3 d_{n,R} \\ & + \Gamma^e_{mn}\bar{l}_{m,L}\phi_3 e_{n,R} + \Gamma^\nu_{mn}\bar{l}_{m,L}\tilde{\phi}_3\nu_{n,R} + \mathrm{H.c.} \end{aligned} \tag{6}$$

We assume the vacuum alignment $\langle\phi_1\rangle = \langle\phi_2\rangle = 0$ and $\langle\phi_3\rangle \neq 0$, so that the Z_3 symmetry is unbroken when EWSB occurs via the Higgs mechanism.

A. The mass eigenstates

We define the components of each doublet as

$$\phi_1 = \begin{pmatrix} H_1^{0+} \\ \frac{H_1^0 + iA_1^0}{\sqrt{2}} \end{pmatrix}, \quad \phi_2 = \begin{pmatrix} H_2^{0+} \\ \frac{H_2^0 + iA_2^0}{\sqrt{2}} \end{pmatrix}, \quad \phi_3 = \begin{pmatrix} H_3^{0+} \\ \frac{v + H_3^0 + iA_3^0}{\sqrt{2}} \end{pmatrix}. \tag{7}$$

The vacuum condition that the point $(\phi_1^0, \phi_2^0, \phi_3^0) = (0, 0, \frac{v}{\sqrt{2}})$ becomes the minimum of the potential leads to the relation

$$v^2 = \frac{\mu_3^2}{\lambda_{33}}. \tag{8}$$

Expanding the potential around this vacuum point results in the mass spectrum below, where the pairs of scalar/pseudoscalar base fields $(H_{1,2}^0/A_{1,2}^0)$ from the inert doublets in Eq. (7) are rotated by

$$R_{\theta_i} = \begin{pmatrix} \cos\theta_i & \sin\theta_i \\ -\sin\theta_i & \cos\theta_i \end{pmatrix}, \tag{9}$$

where $\theta_i = \theta_h, \theta_a$ are the rotation angles for the scalar and pseudoscalar matrices, respectively while there is no mixing between the charged states. The mass spectrum of all spin-0 particles of the I$(2+1)$HDM is presented below.

CP-even scalars:

$$\begin{aligned} \mathbf{h}: m_h^2 &= 2\mu_3^2 = 2\lambda_{33}v^2 \\ \mathbf{H}_1 &= \cos\theta_h H_1^0 + \sin\theta_h H_2^0 \\ m_{H_1}^2 &= \cos^2\theta_h(-\mu_1^2 + \Lambda_1) + \sin^2\theta_h(-\mu_2^2 + \Lambda_2) \\ &\quad + \sin\theta_h\cos\theta_h\lambda_3 v^2 \\ \mathbf{H}_2 &= -\sin\theta_h H_1^0 + \cos\theta_h H_2^0 \\ m_{H_2}^2 &= \sin^2\theta_h(-\mu_1^2 + \Lambda_1) + \cos^2\theta_h(-\mu_2^2 + \Lambda_2) \\ &\quad - \sin\theta_h\cos\theta_h\lambda_3 v^2 \end{aligned}$$

$$\text{with} \quad \Lambda_1 = \frac{1}{2}(\lambda_{31} + \lambda'_{31})v^2, \qquad \Lambda_2 = \frac{1}{2}(\lambda_{23} + \lambda'_{23})v^2,$$

$$\tan 2\theta_h = \frac{-\lambda_3 v^2}{\mu_1^2 - \Lambda_1 - \mu_2^2 + \Lambda_2} \tag{10}$$

CP-odd scalars:

$$\begin{aligned}
\mathbf{A}_1 &= \cos\theta_a A_1^0 + \sin\theta_a A_2^0 \\
m^2_{A_1} &= \cos^2\theta_a(-\mu_1^2+\Lambda_1) + \sin^2\theta_a(-\mu_2^2+\Lambda_2) \\
&\quad - \sin\theta_a\cos\theta_a\lambda_3 v^2 \\
\mathbf{A}_2 &= -\sin\theta_a A_1^0 + \cos\theta_a A_2^0 \\
m^2_{A_2} &= \sin^2\theta_a(-\mu_1^2+\Lambda_1) + \cos^2\theta_a(-\mu_2^2+\Lambda_2) \\
&\quad + \sin\theta_a\cos\theta_a\lambda_3 v^2
\end{aligned}$$

$$\text{with} \quad \tan 2\theta_a = \frac{\lambda_3 v^2}{\mu_1^2 - \Lambda_1 - \mu_2^2 + \Lambda_2} \tag{11}$$

Charged scalars:

$$\begin{aligned}
\mathbf{H}_1^\pm &= H_1^{0\pm}, \qquad m^2_{H_1^\pm} = -\mu_1^2 + \frac{1}{2}\lambda_{31} v^2 \\
\mathbf{H}_2^\pm &= H_2^{0\pm}, \qquad m^2_{H_2^\pm} = -\mu_2^2 + \frac{1}{2}\lambda_{23} v^2.
\end{aligned} \tag{12}$$

Note that $\tan\theta_a = -\tan\theta_h$ and the *CP*-even and *CP*-odd mass eigenstates can be written as

$$\begin{cases} \mathbf{H}_1 \equiv \cos\theta_h H_1^0 + \sin\theta_h H_2^0 \\ \mathbf{H}_2 = -\sin\theta_h H_1^0 + \cos\theta_h H_2^0 \end{cases} \quad \text{and}$$

$$\begin{cases} \mathbf{A}_1 \equiv \cos\theta_h A_1^0 - \sin\theta_h A_2^0 \\ \mathbf{A}_2 = \sin\theta_h A_1^0 + \cos\theta_h A_2^0 \end{cases} \tag{13}$$

with masses

$$\begin{aligned}
m^2_{H_1} = m^2_{A_1} &= \cos^2\theta_h(-\mu_1^2+\Lambda_1) + \sin^2\theta_h(-\mu_2^2+\Lambda_2) \\
&\quad + \sin\theta_h\cos\theta_h\lambda_3 v^2 \\
m^2_{H_2} = m^2_{A_2} &= \sin^2\theta_h(-\mu_1^2+\Lambda_1) + \cos^2\theta_h(-\mu_2^2+\Lambda_2) \\
&\quad - \sin\theta_h\cos\theta_h\lambda_3 v^2.
\end{aligned} \tag{14}$$

Note that the degenerate fields H_1 and A_1 can be grouped together into a complex neutral field $N_1 = (H_1 + iA_1)/\sqrt{2}$ [and H_2 and A_2 states into $N_2 = (H_2 + iA_2)/\sqrt{2}$, correspondingly]. When $\lambda_3 = 0$, the inert doublets decouple from each other and the complex fields N_1 and N_2 become eigenstates of the Z_3 symmetry, with the Z_3 charge $+1$ for N_1 and the Z_3 charge -1 for N_2. In general, though, when $\lambda_3 \neq 0$, the states N_1 and N_2 do not have defined Z_3 quantum numbers. We will discuss this further in Sec. VI where we introduce the concept of hermaphrodite DM and discuss how it is distinguishable from a complex DM scenario.

TABLE I. Angular dependence of (pseudo)scalar-gauge couplings in the Z_3 symmetric model.

Vertex	Vertex coefficient
ZH_iA_i	$\cos 2\theta_h$
ZH_iA_j	$\sin 2\theta_h$
$W^\pm H_i^\mp H_i$	$\cos\theta_h$
$W^\pm H_i^\mp H_j$	$\sin\theta_h$
$W^\pm H_i^\mp A_i$	$\cos\theta_h$
$W^\pm H_i^\mp A_j$	$\sin\theta_h$

We take the mass-degenerate H_1 and A_1 particles as constituents of the hermaphrodite DM state, which are protected from decaying to SM particles through the unbroken Z_3 symmetry. Moreover, the only fields that transform trivially under the Z_3 symmetry are the SM fields and the fields from the only active scalar doublet, ϕ_3, which plays the role of the SM Higgs doublet.

The (pseudo)scalar-gauge boson interaction plays an important role here, since a nonzero H_1A_1Z vertex predicts a signal at direct detection experiments which contradicts the observation and rules out the model as a viable DM framework. As we have shown in Table I, the ZH_1A_1 vertex is proportional to $\cos 2\theta_h$. This vertex vanishes at the $\theta_h = \pi/4$ slice of the parameter space which is where we define our benchmark scenarios in the upcoming sections.

B. Input parameters

We write the parameters of the potential that are relevant for our numerical studies,

$$\begin{aligned}
&\mu_1^2, \quad \mu_2^2, \quad \lambda_{23}, \quad \lambda_{31}, \quad \lambda'_{23}, \quad \lambda'_{31}, \\
&\lambda_3, \quad \lambda_1, \quad \lambda_2
\end{aligned} \tag{15}$$

in terms of physical quantities

$$\begin{aligned}
&m_{H_1}, \quad m_{H_2}, \quad m_{H_1^\pm}, \quad m_{H_2^\pm}, \quad \theta_h, \\
&g_1, \quad g_2, \quad \lambda_1, \quad \lambda_2,
\end{aligned} \tag{16}$$

where $g_1 = g_{hH_1H_1}/v$ and $g_2 = g_{hH_1H_2}/v$ and λ_1 and λ_2 which appear in the cubic inert scalar interactions. The conversion relations are as follows:

$$
\begin{aligned}
\lambda_3 &= \frac{4\sin(2\theta_h)(m_{H_2}^2 - m_{H_1}^2)}{v^2(\cos(4\theta_h) - 3)},\\
\lambda'_{23} &= \frac{2\cos(2\theta_h)(m_{H_1}^2 - m_{H_2}^2)}{v^2(\cos(4\theta_h) - 3)} + \frac{1}{v^2}(m_{H_1}^2 + m_{H_2}^2 - 2m_{H_2^\pm}^2),\\
\lambda'_{31} &= \frac{2\cos(2\theta_h)(m_{H_2}^2 - m_{H_1}^2)}{v^2(\cos(4\theta_h) - 3)} + \frac{1}{v^2}(m_{H_1}^2 + m_{H_2}^2 - 2m_{H_1^\pm}^2),\\
\mu_1^2 &= \frac{-1}{2(\cos(4\theta_h) - 3)}(\cos(4\theta_h)(-g_1 v^2 + m_{H_1}^2 + m_{H_2}^2) + 3g_1 v^2\\
&\quad + g_2 v^2(-2\sin(2\theta_h) + \sin(4\theta_h) - 2\tan(\theta_h)) + 2\cos(2\theta_h)(m_{H_1}^2 - m_{H_2}^2) - 7m_{H_1}^2 + m_{H_2}^2),\\
\mu_2^2 &= \frac{-2}{4(\cos(4\theta_h) - 3)}(\cos(4\theta_h)(-g_1 v^2 + m_{H_1}^2 + m_{H_2}^2) + 3g_1 v^2 + 2g_2 v^2(\cot(\theta_h) + 4\sin(\theta_h)\cos^3(\theta_h))\\
&\quad - 7m_{H_1}^2 + m_{H_2}^2 - 2\cos(2\theta_h)(m_{H_1}^2 - m_{H_2}^2)),\\
\lambda_{23} &= \frac{-1}{v^2(\cos(4\theta_h) - 3)}(\cos(4\theta_h)(-g_1 v^2 + m_{H_1}^2 - 2m_{H_2^\pm}^2 + m_{H_2}^2) + 3g_1 v^2 + 6m_{H_2^\pm}^2 + 2g_2 v^2(\cot(\theta_h) + 4\sin(\theta_h)\cos^3(\theta_h))\\
&\quad + 2\cos(2\theta_h)(m_{H_2}^2 - m_{H_1}^2) - 7m_{H_1}^2 + m_{H_2}^2),\\
\lambda_{31} &= \frac{1}{v^2(\cos(4\theta_h) - 3)}(\cos(4\theta_h)(g_1 v^2 + 2m_{H_1^\pm}^2 - m_{H_1}^2 - m_{H_2}^2) - 3g_1 v^2 - 6m_{H_1^\pm}^2\\
&\quad + g_2 v^2(2\sin(2\theta_h) - \sin(4\theta_h) + 2\tan(\theta_h)) + 2\cos(2\theta_h)(m_{H_2}^2 - m_{H_1}^2) + 7m_{H_1}^2 - m_{H_2}^2).
\end{aligned}
\tag{17}
$$

III. CONSTRAINTS ON THE MODEL PARAMETERS

As the third doublet is identified with the SM Higgs doublet, μ_3, λ_{33} are Higgs field parameters, renormalized by the Higgs mass. We use the value $m_h = 125$ GeV for the latter, so that

$$m_h^2 = 2\mu_3^2 = 2\lambda_{33}v^2. \tag{18}$$

For the V_0 part of the potential to have a stable vacuum (bounded from below) [16,17], the following conditions are required[4]:

$$
\begin{aligned}
&\lambda_{11}, \lambda_{22}, \lambda_{33} \geq 0,\\
&\widetilde{\lambda_{12}} \equiv \lambda_{12} + \lambda'_{12} + \sqrt{\lambda_{11}\lambda_{22}} \geq 0,\\
&\widetilde{\lambda_{23}} \equiv \lambda_{23} + \lambda'_{23} + \sqrt{\lambda_{22}\lambda_{33}} \geq 0,\\
&\widetilde{\lambda_{31}} \equiv \lambda_{31} + \lambda'_{31} + \sqrt{\lambda_{33}\lambda_{11}} \geq 0,\\
&\sqrt{\lambda_{11}\lambda_{22}\lambda_{33}} + (\lambda_{12} + \lambda'_{12})\sqrt{\lambda_{33}} + (\lambda_{31} + \lambda'_{31})\sqrt{\lambda_{22}}\\
&+ (\lambda_{23} + \lambda'_{23})\sqrt{\lambda_{11}} + \sqrt{2\widetilde{\lambda_{12}}\,\widetilde{\lambda_{31}}\,\widetilde{\lambda_{23}}} \geq 0.
\end{aligned}
\tag{19}
$$

[4]These conditions emerge from requiring the quartic part of the potential to be positive as the fields $\phi_i \to \infty$. The "copositivity" method suggested in [22] will result in more restrictive constraints.

We also require the parameters of the V_{Z_3} part to be smaller than the parameters of the V_0 part:

$$|\lambda_1|, |\lambda_2|, |\lambda_3| < |\lambda_{ii}|, |\lambda_{ij}|, |\lambda'_{ij}|, \qquad i \neq j = 1, 2, 3, \tag{20}$$

so that they do not dominate the behavior of the potential at high field values. For the point $(0, 0, \frac{v}{\sqrt{2}})$ to be the minimum of the potential, the mass eigenvalues must be positive. Therefore, it is required that

$$
\begin{aligned}
&-\mu_1^2 + \lambda_{31}\frac{v^2}{2} > 0,\\
&-\mu_2^2 + \lambda_{23}\frac{v^2}{2} > 0,\\
&-2(\mu_1^2 + \mu_2^2) + v^2(\lambda_{23} + \lambda'_{23} + \lambda_{31} + \lambda'_{31})\\
&\quad > |2(\mu_1^2 - \mu_2^2) + v^2(\lambda_{23} + \lambda'_{23} - \lambda_{31} - \lambda'_{31})|,
\end{aligned}
\tag{21}
$$

which also renders the $(0, 0, \frac{v}{\sqrt{2}})$ point the global minimum of the potential. From the S-matrix unitarity for elastic scattering of 2-to-2 body bosonic states, the magnitude of combinations of the λ parameters in the potential is constrained. In agreement with perturbativity bounds, we take the absolute values $|\lambda_i| \leq 2\pi$ which also satisfies the unitarity conditions in [23].

Measurements done at Large Electron-Positron Collider (LEP) [24,25] limit the invisible decays of Z and $W^\pm$ gauge bosons, requiring that

$$m_{H_i^\pm} + m_{H_i,A_i} > m_{W^\pm}$$
$$m_{H_i} + m_{A_i} > m_Z$$
$$2m_{H_i^\pm} > m_Z. \tag{22}$$

Also, LEP provides a model-independent lower limit for the mass of the charged scalars:

$$m_{H_i^\pm} > 70\text{–}90 \text{ GeV}. \tag{23}$$

Searches for charginos and neutralinos at LEP have been translated into limits of region of masses in the I(1 + 1)HDM [25] where for

$$m_H < 80 \text{ GeV} \quad \text{and} \quad m_A < 100 \text{ GeV}$$

the following region is excluded:

$$m_A - m_H > 8 \text{ GeV}. \tag{24}$$

We have taken this limit into account in our numerical studies for any pair of *CP*-even and *CP*-odd particles.

Finally, the decay width of the Higgs into a pair of the inert scalars with $m_{S_i} < m_h/2$ is

$$\Gamma(h \to S_i S_j) = \frac{g_{hS_iS_j}^2 v^2}{32\pi m_h^3}[(m_h^2 - (m_{S_i} + m_{S_j})^2)(m_h^2 - (m_{S_i} - m_{S_j})^2)]^{1/2}, \tag{25}$$

with $S_i, S_j = H_1, A_1$ where $g_{hS_iS_j}v$ is the coefficient of the hS_iS_j term in the Lagrangian and m_{S_i} is the mass of the corresponding neutral inert particle. Experimental measurements of invisible Higgs decays limit models in which the Higgs boson can decay into lighter particles which escape detection. The current limits on the SM-like Higgs boson invisible (inv) branching ratio (BR) from the ATLAS experiment are [26]

$$\text{BR}(h \to \text{inv}) < 0.08\text{–}0.15. \tag{26}$$

This leads to strong constraints on the Higgs-DM coupling. For our scenarios this BR is

$$\text{BR}(h \to \text{inv}) = \frac{\Sigma_i \Gamma(h \to S_i S_i)}{\Gamma_h^{\text{SM}} + \Sigma_i \Gamma(h \to S_i S_i)}, \tag{27}$$

where $S_i = H_1, A_1$.

Regarding constraints coming from $h \to \gamma\gamma$, the inert charged masses and parameters in our analysis fall within the acceptable ranges obtained in Ref. [14] where a combined ATLAS and CMS run 1 limit was used for the SM-like Higgs signal strengths.

IV. SELECTION OF BENCHMARK SCENARIOS

As discussed before, for mass-degenerate H_1 and A_1 particles to qualify as viable DM candidates, the ZH_iA_i vertex, proportional to $\cos 2\theta_h$ must vanish. Therefore, $\theta_h = \pi/4$ is the only acceptable value in the $0 \le \theta_h < \pi$ range for the model to qualify as a viable DM framework.

With $\theta_h = \pi/4$, the mixing between the inert doublets ϕ_1 and ϕ_2 is maximal and the neutral mass relations are reduced to

$$m_{H_1}^2 = m_{A_1}^2 = -\frac{1}{2}(\mu_1^2 + \mu_2^2) + \frac{v^2}{4}(\lambda_{31} + \lambda'_{31} + \lambda_{23} + \lambda'_{23} + 2\lambda_3),$$
$$m_{H_2}^2 = m_{A_2}^2 = -\frac{1}{2}(\mu_1^2 + \mu_2^2) + \frac{v^2}{4}(\lambda_{31} + \lambda'_{31} + \lambda_{23} + \lambda'_{23} - 2\lambda_3). \tag{28}$$

The charged mass eigenstates are as presented in Eq. (12). In this limit the relations for the parameters in terms of the observables also reduce to

$$\lambda_{23} = \frac{1}{v^2}(g_1 v^2 + g_2 v^2 - 2m_{H_1}^2 + 2m_{H_2^\pm}^2),$$
$$\lambda_{31} = \frac{1}{v^2}(g_1 v^2 - g_2 v^2 + 2m_{H_1^\pm}^2 - 2m_{H_1}^2),$$
$$\lambda'_{23} = \frac{1}{v^2}(m_{H_1}^2 - 2m_{H_2^\pm}^2 + m_{H_2}^2),$$
$$\lambda'_{31} = \frac{1}{v^2}(m_{H_1}^2 - 2m_{H_1^\pm}^2 + m_{H_2}^2),$$
$$\mu_1^2 = \frac{1}{2}(g_1 v^2 - g_2 v^2 - 2m_{H_1}^2), \quad \mu_2^2 = \frac{1}{2}(g_1 v^2 + g_2 v^2 - 2m_{H_1}^2),$$
$$\lambda_3 = \frac{1}{v^2}(m_{H_1}^2 - m_{H_2}^2). \tag{29}$$

Taking all constraints discussed into account, we devise the following benchmark scenarios in the $\theta_h = \pi/4$ limit, using the notation

$$\Delta_n = m_{H_2} - m_{H_1}, \qquad \Delta_c = m_{H_1^\pm} - m_{H_1},$$
$$\delta_c = m_{H_2^\pm} - m_{H_1^\pm}. \tag{30}$$

In the low mass region ($45 \text{ GeV} \le m_{\text{DM}} = m_{H_1} = m_{A_1} \le 100 \text{ GeV}$), using the nomenclature in accordance to the Z_2 symmetric I(2 + 1)HDM literature [11,12], we define two benchmark scenarios:

(i) B-type scenarios with $\Delta_n = 50$ GeV, $\Delta_c = 60$ GeV and $\delta_c = 10$ GeV:

$$m_{H_1} = m_{A_1} \ll m_{A_2} = m_{H_2} \ll m_{H_1^\pm} \sim m_{H_2^\pm}, \tag{31}$$

where all other inert particles are much heavier than the mass-degenerate DM constituents H_1 and A_1 and therefore cannot coannihilate with them. Also, due to the absence of the ZH_1A_1 coupling there is no Z mediated coannihilation between H_1 and A_1.

TABLE II. Input parameter values for the benchmark scenario scans in Figs. 4–6.

			Scenario B	Scenario C	Scenario G
$\lambda_{11} = 0.13$	$\lambda'_{12} = 0.12$	$-0.2 < g_1 < 0.2$	$\Delta_n = 50$ GeV	$\Delta_n = 10$ GeV	$\Delta_n = 2$ GeV
$\lambda_{22} = 0.11$	$\lambda_1 = 0.1$	$-0.2 < g_2 < 0.2$	$\Delta_c = 60$ GeV	$\Delta_c = 50$ GeV	$\Delta_c = 0.8$ GeV
$\lambda_{12} = 0.12$		$-0.1 < \lambda_2 < 0.1$	$\delta_c = 10$ GeV	$\delta_c = 1$ GeV	$\delta_c = 0.5$ GeV

Moreover, CP conservation forbids the coupling hH_1A_1 and as a result, there are no Higgs mediated coannihilation modes between H_1 and A_1. The only annihilation processes are through H_1H_1h and A_1A_1h vertices.

(ii) C-type scenarios with $\Delta_n = 10$ GeV, $\Delta_c = 50$ GeV and $\delta_c = 1$ GeV:

$$m_{H_1} = m_{A_1} \sim m_{A_2} = m_{H_2} \ll m_{H_1^\pm} \sim m_{H_2^\pm}, \quad (32)$$

where H_1 and A_1 are close in mass with other neutral inert particles and could coannihilate through Higgs and Z mediated processes.

For the heavy mass region, $m_{\rm DM} > 100$ GeV, there is only one benchmark scenario that is realizable here referred to as the G-type one, using the nomenclature of the Z_2 symmetric I$(2+1)$HDM literature.[5]

(i) G-type scenario with $\Delta_n = 2$ GeV, $\Delta_c = 0.8$ GeV and $\delta_c = 0.5$ GeV:

$$m_{H_1} = m_{A_1} \sim m_{A_2} = m_{H_2} \sim m_{H_1^\pm} \sim m_{H_2^\pm}, \quad (33)$$

where H_1 and A_1 are close in mass with all other inert particles and could coannihilate through Higgs, Z and $W^\pm$ mediated processes.

In Table II, we show the input parameter values that we have used in our numerical analysis, which satisfy all constraints discussed in the previous section. Our numerical analysis shows that H_1 and A_1 contribute identically to the DM relic density with identical cross sections and interactions. The production and annihilation processes for the two constituents of DM, H_1 and A_1, are proportional to H_1H_1h, A_1A_1h and H_1H_1VV, A_1A_1VV couplings which are identical for H_1 and A_1. Therefore H_1 and A_1 contribute identically to the DM relic density with identical cross sections and interactions. Our analysis also confirms that varying inert self-interaction vertices (proportional to the λ_1 and λ_2 parameters),

$$g_{H_1A_1A_1} = -\frac{3}{2\sqrt{2}}(\lambda_1+\lambda_2)v, \quad g_{H_2A_2A_2} = -\frac{3}{2\sqrt{2}}(\lambda_1-\lambda_2)v, \quad (34)$$

$$g_{H_1A_2A_2} = \frac{1}{2\sqrt{2}}(\lambda_1+\lambda_2)v, \quad g_{H_2A_1A_1} = \frac{1}{2\sqrt{2}}(\lambda_1-\lambda_2)v, \quad (35)$$

$$g_{H_1A_2A_1} = -\frac{1}{2\sqrt{2}}(\lambda_1-\lambda_2)v, \quad g_{H_2A_2A_1} = -\frac{1}{2\sqrt{2}}(\lambda_1+\lambda_2)v, \quad (36)$$

does not affect the tree-level DM and collider phenomenology of the model.

Allowing for different values of g_1 and g_2, we present in Figs. 1–3 the combined relic density of the mass-degenerate constituents of DM, H_1 and A_1, with respect to $m_{\rm DM}$ ($m_{\rm DM} = m_{H_1} = m_{A_1}$) for benchmark scenarios B, C and G. Our analysis shows that, in all scenarios, varying g_2, the coefficient of the hH_1H_2 vertex, does not affect the behavior of the model, while varying g_1, the coefficient of the hH_1H_1 vertex, dictates the relic density of DM. For scenarios B and C, for a given g_1, the model overproduces DM for masses below 50 GeV, while DM is underproduced in the vicinity of the Higgs resonance region ($m_h/2 \approx 62$ GeV). For larger $m_{\rm DM}$, for a given g_1, DM is again overproduced until we hit the $W^\pm$ and Z resonances and DM production is suppressed.

V. RESULTS

A. DM relic density

As a reference value, we use the DM relic abundance measured by Planck [27]:

$$\Omega_{\rm DM}h^2 = 0.1198 \pm 0.0027. \quad (37)$$

Due to the presence of two constituents of DM, H_1 and A_1, the prediction of the total relic density is given by

$$\Omega_{\rm DM}h^2 = \Omega_{H_1}h^2 + \Omega_{A_1}h^2. \quad (38)$$

For the numerical evaluation of the relic abundance, we use micrOMEGAs [28] to show the behavior of our benchmark scenarios B and C defined in Sec. IV.

In Figs. 4–6, we show the DM mass versus the Higgs-DM coupling and highlight the regions where the model

[5]The benchmark scenario H defined for the heavy mass region in the Z_2 symmetric I$(2+1)$HDM, with the second inert family split from the first inert family, is not realizable in the Z_3 symmetric I$(2+1)$HDM. This is due to the construction of the model which does not allow for a large mass splitting between the two charged inert states $H_1^\pm$ and $H_2^\pm$.

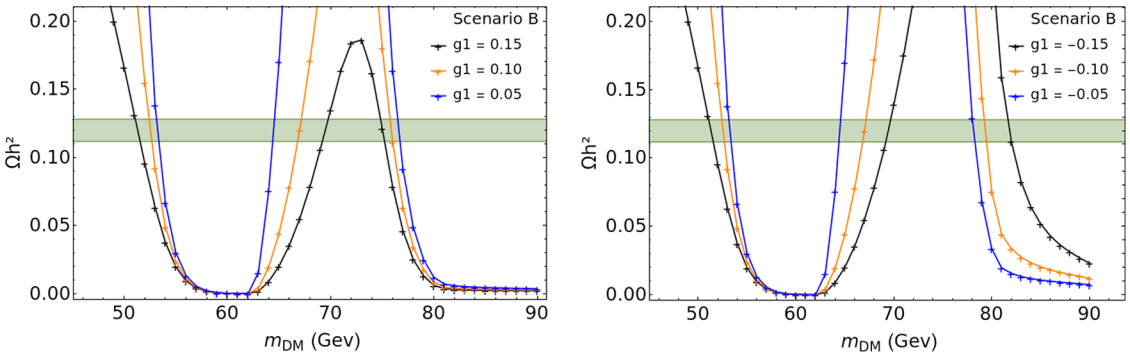

FIG. 1. The combined relic density of the DM constituents H_1 and A_1 with respect to m_{DM} in benchmark scenario B for varying values of positive (left) and negative (right) g_1 coupling. The green band represents the DM observed relic density within 3σ.

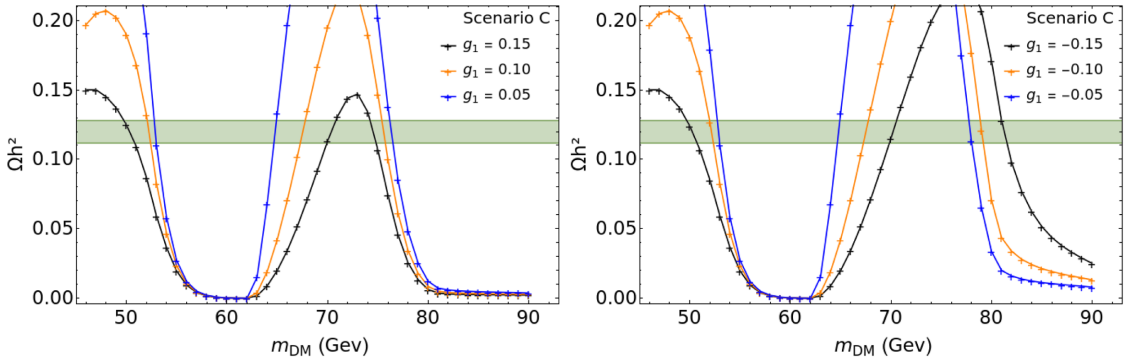

FIG. 2. The combined relic density of the DM constituents H_1 and A_1 with respect to m_{DM} in benchmark scenario C for varying values of positive (left) and negative (right) g_1 coupling. The green band represents the DM observed relic density within 3σ.

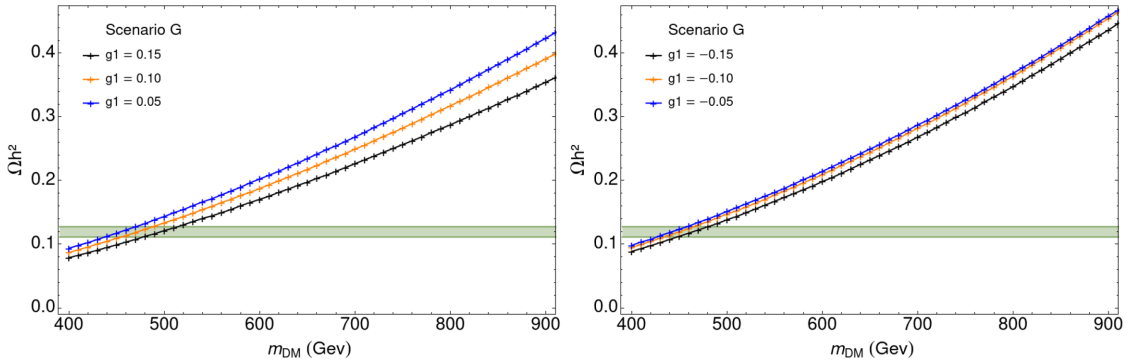

FIG. 3. The combined relic density of the DM constituents H_1 and A_1 with respect to m_{DM} in benchmark scenario G for varying values of positive (left) and negative (right) g_1 coupling. The green band represents the DM observed relic density within 3σ.

produces the DM relic density in 3σ agreement with Eq. (38). The gray regions represent areas where DM (co)annihilation is not strong enough and, as a result, DM is overproduced. These regions are therefore ruled out by Planck observations. The unshaded regions are where DM is underproduced. Note that due to the presence of coannihilation channels, in scenario C a more extensive range of Higgs-DM coupling produces the sufficient amount of DM; hence, the blue band is thicker for scenario C in Fig. 5 compared to the green band for scenario B in Fig. 4. In scenario G, where the charged inert scalars also coannihilate with the DM particles, the violet band showing the region with correct relic density is even broader as shown in Fig. 6.

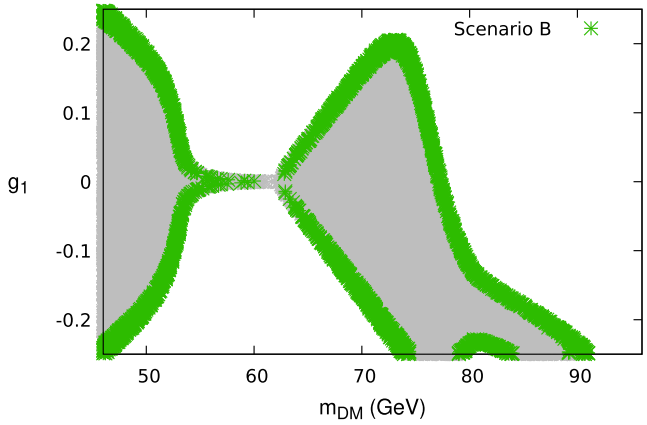

FIG. 4. Regions where the model produces the DM relic density in 3σ agreement with Eq. (38) in the DM mass vs Higgs-DM coupling plane in green for scenario B for the input values in Table II. The gray region represents areas where DM (co)annihilation is not strong enough and, as a result, DM is overproduced. The unshaded regions are where DM is underproduced.

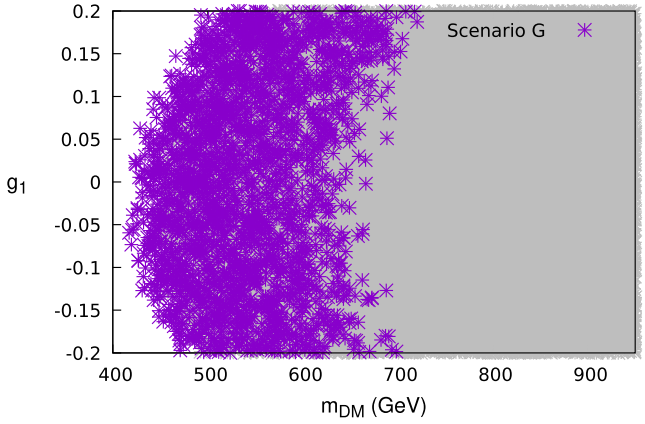

FIG. 6. Regions where the model produces the DM relic density in 3σ agreement with Eq. (38) in the DM mass vs Higgs-DM coupling plane in violet for scenario G for the input values in Table II. The gray region represents areas where DM (co)annihilation is not strong enough and, as a result, DM is overproduced. The unshaded regions are where DM is underproduced.

For both scenarios B and C, in the light DM mass region, the plots are symmetric for positive and negative g_1 values since the cross section of the Higgs mediated annihilation process $H_1H_1/A_1A_1 \to h \to f\bar{f}$ is proportional to g_1^2. In the vicinity of the Higgs resonance region, the $H_1H_1/A_1A_1 \to h$ process is very efficient and reduces the DM abundance significantly, so much so that the Higgs-DM coupling g_1 has to take very small values. Recall also from Figs. 1 and 2 that, for $m_{\rm DM} \sim m_h/2$, even negligible values of g_1 lead to the underproduction of DM. The main annihilation channels in this mass region are the $H_1H_1/A_1A_1 \to b\bar{b}$ process contributing ∼28% and the

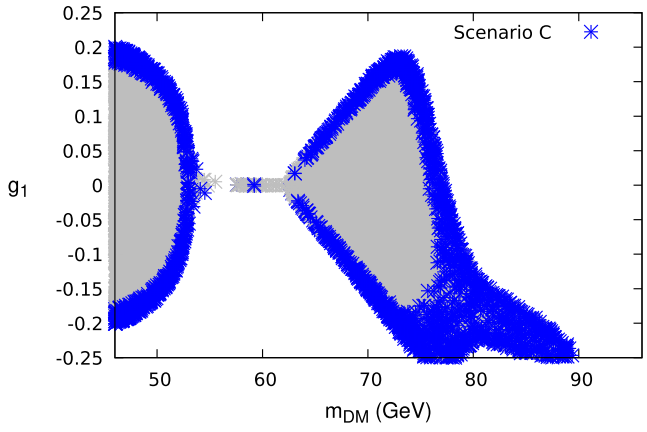

FIG. 5. Regions where the model produces the DM relic density in 3σ agreement with Eq. (38) in the DM mass vs Higgs-DM coupling plane in blue for scenario C for the input values in Table II. The gray region represents areas where DM (co)annihilation is not strong enough and, as a result, DM is overproduced. The unshaded regions are where DM is underproduced.

$H_1H_1/A_1A_1 \to W^{+*}W^{-*}$ process contributing ∼14% of the annihilation cross section (with other annihilation channels individually subdominant). As the DM mass increases, the contribution from the $b\bar{b}$ process reduces while the contribution from the $W^{+*}W^{-*}$ process grows, reaching ∼50% of the total annihilation cross section for $m_{\rm DM} \sim m_{W^\pm}$. In the heavier mass region, the point annihilation channel $H_1H_1/A_1A_1 \to W^\pm W^\mp$ opens up and interferes destructively with the Higgs mediated process $H_1H_1/A_1A_1 \to h \to W^\pm W^\mp$. For larger values of DM mass the point annihilation is stronger, and a larger Higgs-DM coupling is required for the effective cancellation of the $H_1H_1/A_1A_1 \to W^\pm W^\mp$ process. This results in larger negative values of the Higgs-DM coupling in this region. For heavier DM masses, above m_Z, the annihilation to gauge bosons is so strong that DM is always underproduced regardless of the value of the Higgs-DM coupling. This is a common pattern in inert doublet models of DM, such as the I(1 + 2)HDM and the Z_2 symmetric I(2 + 1)HDM.

For much heavier DM masses, where charged inert particles are also close in mass with the DM states, the destructive interference of all coannihilation processes leads to a sufficient relic density of DM, as represented by scenario G. The behavior of the model is similar to the Z_2 symmetric case studied in Ref. [18], wherein, in order to get the correct relic density, larger Δ_c values require larger negative Higgs-DM couplings, smaller Δ_n values require lower DM masses and larger δ_c values weaken the coannihilation effects and shrink the violet band.

B. Direct and indirect detection limits

DM direct detection experiments measure the scattering of DM particles off nuclei. This interaction is mediated by

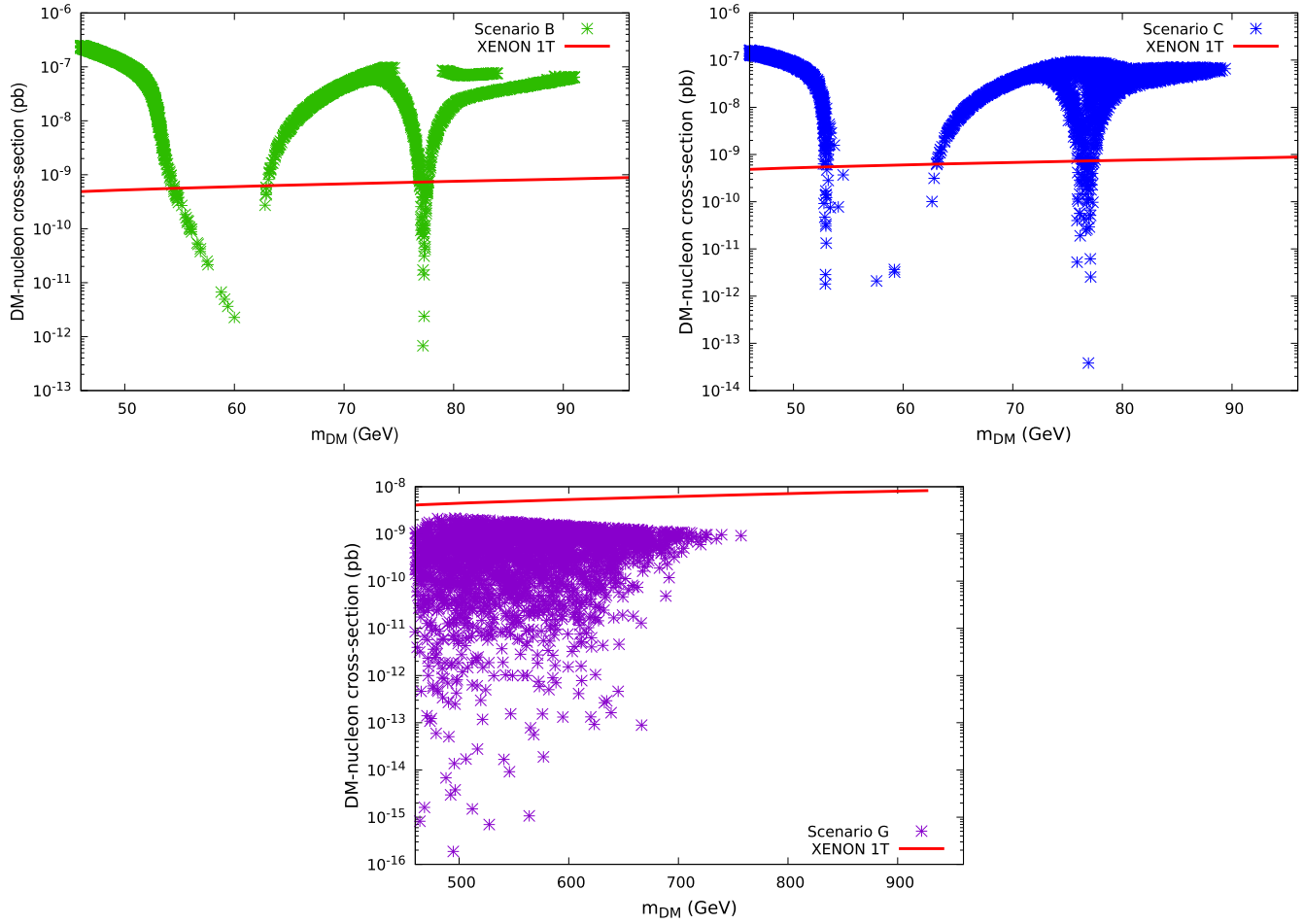

FIG. 7. Direct detection bounds on the points that saturate the relic density for scenarios B (top left), C (top right) and G (bottom). The solid red line corresponds to the current XENON1T limit above which any point is ruled out.

the Higgs or Z boson; therefore results of these experiments constrain the DM mass, as well as the Higgs-DM coupling, g_1, and the ZH_1A_1 coupling. As discussed in detail before, we study a region of the parameter space where the ZH_1A_1 coupling is zero which is a consequence of the exact Z_3 symmetry of the model and the choice of $\theta_h = \pi/4$.

Figure 7 shows the direct detection bounds on the points that saturate the relic density for scenarios B, C and G, where the solid red line corresponds to the current XENON1T limit [29], therefore any point above this line is ruled out. In connection with the plots in Figs. 4 and 5, note that when the Higgs-DM coupling tends to zero, the direct detection cross section in Fig. 7 is reduced to values well below the limit from XENON1T. In the top panels, the two branches of direct detection cross section in the large mass region of the plots correspond to the two asymmetric relic density bands in Figs. 4 and 5 with different Higgs-DM coupling values. The direct detection search by XENON1T does not exclude any relevant point in scenario G.

Indirect detection results from Fermi Large Area Telescope [30] strongly constrain DM annihilation into $b\bar{b}$ and $\tau^+\tau^-$. Figure 8 shows the indirect detection bounds on the points that saturate the relic density for scenarios B, C and G, where the solid red line corresponds to the current Fermi Large Area Telescope limit above which any point is ruled out. In the top panels, the two branches of indirect detection cross section correspond to two asymmetric relic density bands in Figs. 4 and 5 with different Higgs-DM coupling values. Notice that indirect detection bounds are much less constraining than the direct detection ones, with almost all points in scenarios B, C and G in agreement with the Fermi Large Area Telescope bounds.

To summarize this section, in Fig. 9, we show the effect of the constraints in the $[m_{\rm DM}, g_1]$ plane for scenarios B and C. In red, we show the region of the parameter space excluded by direct detection bounds from XENON1T presented in Fig. 7, which are more constraining that the indirect detection bounds from Fermi Large Area Telescope as shown in Fig. 8. The blue shaded regions are excluded by the Higgs invisible BR limits as discussed in Eqs. (25)–(27). The points producing the correct relic density for scenarios B and C are shown in green and blue, respectively, in 3σ agreement with Eq. (38). In the heavy mass region, all points in scenario G leading to the correct DM

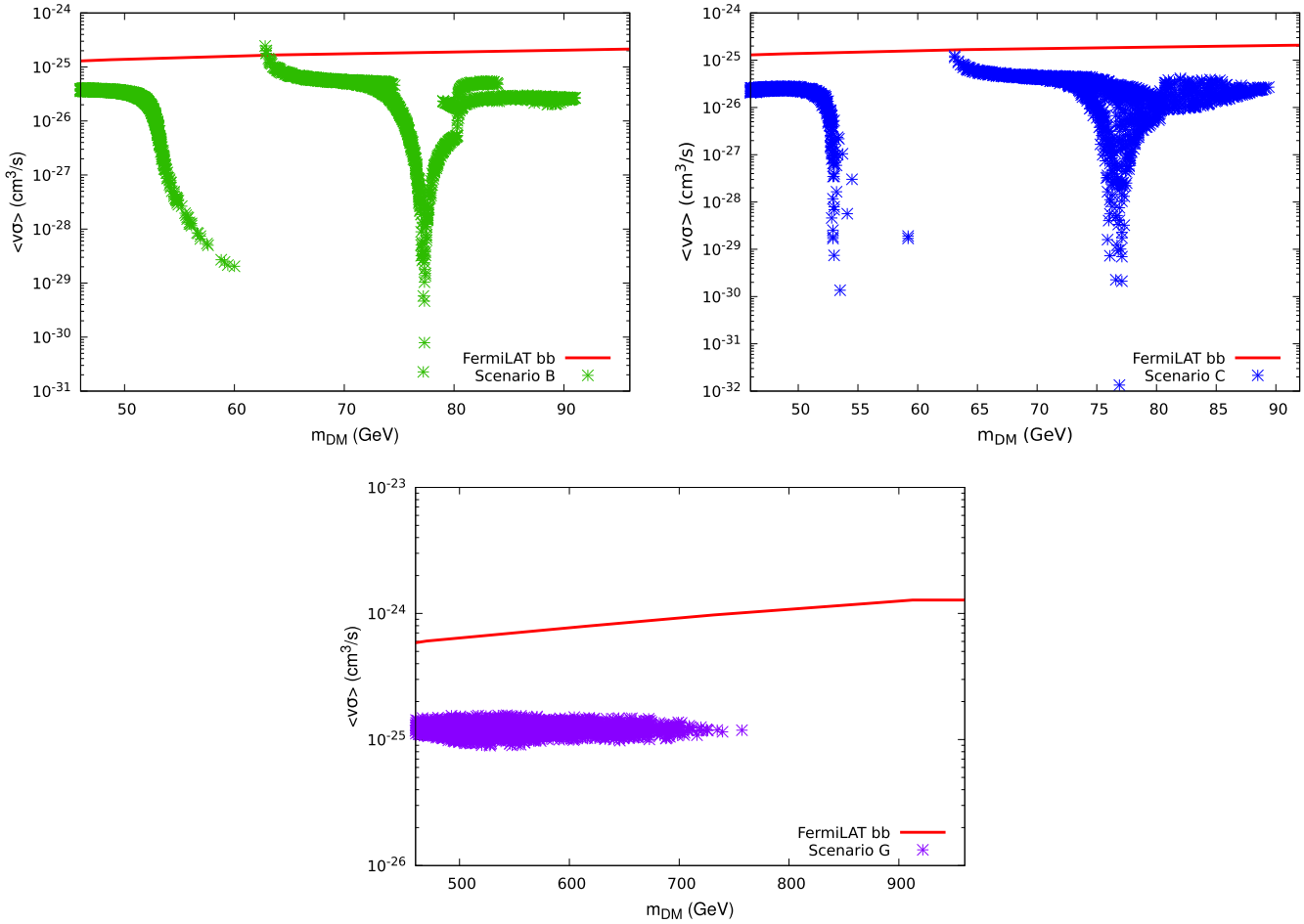

FIG. 8. Indirect detection bounds on the points that saturate the relic density for scenarios B (top left), C (top right) and G (bottom). The solid red line corresponds to the current Fermi Large Area Telescope limit above which any point is ruled out.

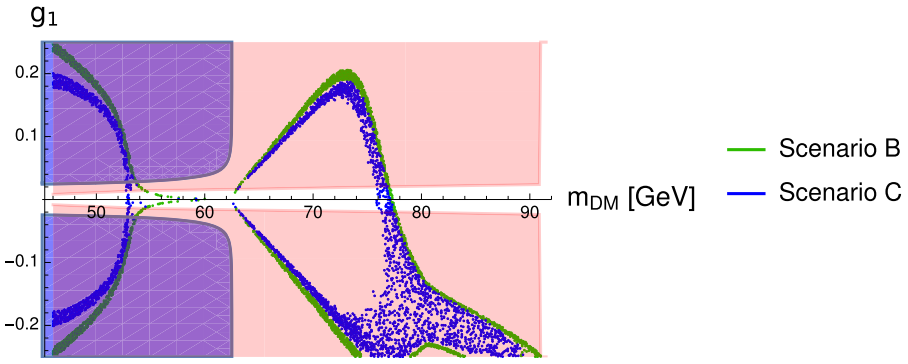

FIG. 9. The effect of the experimental constraints on the parameter space of benchmark scenarios B and C in the $m_{\rm DM}$, g_1 plane. The red-shaded regions are excluded by direct and indirect detection experiments while blue-shaded regions are excluded by the Higgs invisible branching ration bounds.

relic density satisfy both direct and indirect detection bounds.

We could compare our results with those obtained in Ref. [31], wherein a Z_3 symmetric I$(1 + 1)$HDM plus inert singlet is explored. In their analysis, they do not have points satisfying XENON1T limits for DM masses below 300 GeV. The latter would mean that adding a doublet to the I$(1 + 1)$HDM, rather than a singlet scalar, has the advantage of opening up regions for the low mass range in the DM mass.

VI. HERMAPHRODITE DM SCENARIO

As mentioned before, the $\theta_h = \pi/4$ limit is the only viable limit for H_1 and A_1 as the two constituents of DM in the exact Z_3 symmetric configuration. In this case, the masses of H_1 and A_1 are degenerate and the gauge coupling ZH_1A_1 vanishes. In terms of DM phenomenology, this scenario naively appears to be identical to a DM model with one complex scalar field $N = H_1 + iA_i$, rather than a DM with two constituents. In fact, the relevant couplings to the annihilation of the DM particles in the early Universe and the DM scattering off nuclei are the same as those in a model with the aforementioned complex scalar DM.

However, once we turn our attention to the various parts of the Lagrangian, we realize that there are several remnants of the Z_3 symmetry of the model. The most interesting one is the $ZH_iA_j(i \neq j)$ interaction, which does not appear in a complex scalar DM model, even if the additional fields A_2 and H_2 or a complex field $N_2 = H_2 + iA_2$ are introduced. Moreover, there are significant differences in the (pseudo)scalar self-interactions. In a model with a complex scalar DM, the triple (pseudo)scalar couplings should have the form $hN^*N = hH_1H_1 + hA_1A_1$, i.e., without symmetry breaking in the dark sector. In contrast, our model has triple dark (pseudo)scalar couplings such as $H_1H_1H_1$ or $H_1A_1A_1$, as shown in Eqs. (34)–(36). (Further note that our scenario does not have couplings such as $A_1A_1A_1$ and $A_1H_1H_1$ because of CP symmetry conservation.) By exploring such interactions at collider experiments such as the high-luminosity LHC (HL-LHC) [32] and/or a future electron-positron collider [33], one can potentially distinguish our scenario from models with a complex scalar DM.

In summary, from the viewpoint of DM physics and collider phenomenology, one cannot identify H_1 and A_1, the two constituents of DM in our scenario, with the real and imaginary parts of one complex scalar DM particle. Indeed, while H_1 and A_1 behave identically as DM constituents, they have an opposite CP parity. For these reasons, we coin the term hermaphrodite DM for such a DM framework with two otherwise identical constituents but opposite CP.

VII. CONCLUSIONS

Motivated by two problems in the SM, from the experimental side, the absence of viable DM candidates, and, from the theoretical side, the lack of an explanation for the three families of matter, we have postulated a 3HDM, wherein two doublets are inert (or dark), and one is active (i.e., with a SM-Higgs nature). This so-called I$(2+1)$HDM version of the 3HDM has been repeatedly studied in the literature and shown to be viable against both theoretical constraints and experimental limits when a Z_2 symmetry is imposed by hand onto the Lagrangian, according to which all SM fields, including the active doublet generating the Z, $W^\pm$ and Higgs masses measured by experiment, are even while all those emerging from the two inert doublets are odd. A consequence of this is that the lightest dark state is a viable DM candidate.

In this paper, we have instead adopted a Z_3 symmetry which, combined with the $(0, 0, v)$ structure for the doublet VEVs leads naturally to a novel phenomenon which we call hermaphrodite DM here. In this setup, two mass-degenerate inert spinless bosons of opposite CP, which are the lightest amongst the dark particles, contribute identically to DM phenomenology. We have then shown that such DM scenario is distinguishable from the complex scalar DM case. Furthermore, all such dynamics have been obtained in the presence of known (in)direct constraints on DM, as well as those stemming from electroweak precision observables and collider data, so that we have produced a phenomenologically successful DM framework based upon a scalar potential and VEV structure which is theoretically well motivated. Finally, as a by-product of this analysis, we have also obtained that compliance with experimental results requires the DM mass to be rather light, in fact, at or below the EW scale. Therefore, this ultimately opens the door to the possibility of producing peculiar signals of these dark states, such as DM clumps, core-cusp dynamics in galactic centers or separate cascade processes terminating with two different DM constituents at the LHC, which will be the subject of an upcoming publication.

ACKNOWLEDGMENTS

S. M. is supported in part through the NExT Institute and STFC Consolidated Grant No. ST/L000296/1. D. R.-C. is supported by the Royal Society Newton International Fellowship NIF/R1/180813. S. M. and D. R.-C. are also partially supported by the H2020-MSCA-RISE-2014 Grant No. 645722 (NonMinimalHiggs). T. S. and S. M. are partially supported by the Kogakuin University Grant for the project research "Phenomenological study of new physics models with extended Higgs sector." A. A. acknowledges support from CONACYT Project No. CB-2015-01/257655 and Sistema Nacional de Investigadores (SNI) (México). V. K. acknowledges financial support from Academy of Finland projects "Particle cosmology and gravitational waves" No. 320123 and "Particle cosmology beyond the Standard Model" No. 310130. J. H.-S. has been supported by SNI-CONACYT (Mexico), Vicerrectoria de Investigacion y Educacion Superior (VIEP)-BUAP and Programa para el Desarrollo Profesional Docente (PRODEP)-SEP (Mexico) under the grant "Red Tematica: Fisica del Higgs y del Sabor." The authors acknowledge the use of the IRIDIS High Performance Computing Facility, and associated support services at the University of Southampton, in the completion of this work.

[1] G. Aad *et al.* (ATLAS Collaboration), Observation of a new particle in the search for the standard model Higgs boson with the ATLAS detector at the LHC, Phys. Lett. B **716**, 1 (2012).

[2] S. Chatrchyan *et al.* (CMS Collaboration), Observation of a new boson at a mass of 125 GeV with the CMS experiment at the LHC, Phys. Lett. B **716**, 30 (2012).

[3] G. C. Branco, P. M. Ferreira, L. Lavoura, M. N. Rebelo, M. Sher, and J. P. Silva, Theory and phenomenology of two-Higgs-doublet models, Phys. Rep. **516**, 1 (2012).

[4] P. A. R. Ade *et al.* (Planck Collaboration), Planck 2013 results. XVI. Cosmological parameters, Astron. Astrophys. **571**, A16 (2014).

[5] N. G. Deshpande and E. Ma, Pattern of symmetry breaking with two Higgs doublets, Phys. Rev. D **18**, 2574 (1978).

[6] I. P. Ivanov and E. Vdovin, Classification of finite reparametrization symmetry groups in the three-Higgs-doublet model, Eur. Phys. J. C **73**, 2309 (2013).

[7] N. Darvishi and A. Pilaftsis, Classifying accidental symmetries in multi-Higgs doublet models, Phys. Rev. D **101**, 095008 (2020).

[8] S. Weinberg, Gauge Theory of *CP* Nonconservation, Phys. Rev. Lett. **37**, 657 (1976).

[9] I. P. Ivanov and V. Keus, Z_p scalar dark matter from multi-Higgs-doublet models, Phys. Rev. D **86**, 016004 (2012).

[10] B. Grzadkowski, O. M. Ogreid, P. Osland, A. Pukhov, and M. Purmohammadi, Exploring the *CP*-violating inert-doublet model, J. High Energy Phys. 06 (2011) 003.

[11] V. Keus, S. F. King, S. Moretti, and D. Sokolowska, Dark matter with two inert doublets plus one Higgs doublet, J. High Energy Phys. 11 (2014) 016.

[12] A. Cordero-Cid, J. Hernandez-Sanchez, V. Keus, S. King, S. Moretti, D. Rojas, and D. Sokolowska, *CP* violating scalar dark matter, J. High Energy Phys. 12 (2016) 014.

[13] A. Cordero-Cid, J. Hernández-Sánchez, V. Keus, S. Moretti, D. Rojas-Ciofalo, and D. Sokołowska, Collider signatures of dark *CP* violation, Phys. Rev. D **101**, 095023 (2020).

[14] A. Cordero-Cid, J. Hernández-Sánchez, V. Keus, S. Moretti, D. Rojas, and D. Sokołowska, Lepton collider indirect signatures of dark *CP*-violation, Eur. Phys. J. C **80**, 135 (2020).

[15] V. Keus, S. F. King, and S. Moretti, Three-Higgs-doublet models: Symmetries, potentials and Higgs boson masses, J. High Energy Phys. 01 (2014) 052.

[16] V. Keus, S. F. King, and S. Moretti, Phenomenology of the inert (2 + 1) and (4 + 2) Higgs doublet models, Phys. Rev. D **90**, 075015 (2014).

[17] F. S. Faro and I. P. Ivanov, Boundedness from below in the $U(1) \times U(1)$ three-Higgs-doublet model, Phys. Rev. D **100**, 035038 (2019).

[18] V. Keus, S. F. King, S. Moretti, and D. Sokolowska, Observable heavy Higgs dark matter, J. High Energy Phys. 11 (2015) 003.

[19] A. Cordero, J. Hernandez-Sanchez, V. Keus, S. F. King, S. Moretti, D. Rojas, and D. Sokolowska, Dark matter signals at the LHC from a 3HDM, J. High Energy Phys. 05 (2018) 030.

[20] A. Aranda, J. Hernández–Sánchez, R. Noriega-Papaqui, and C. A. Vaquera-Araujo, Yukawa textures or dark doublets from two Higgs doublet models with Z_3 symmetry, arXiv:1410.1194.

[21] I. P. Ivanov, V. Keus, and E. Vdovin, Abelian symmetries in multi-Higgs-doublet models, J. Phys. A **45**, 215201 (2012).

[22] K. Kannike, Vacuum stability conditions from copositivity criteria, Eur. Phys. J. C **72**, 2093 (2012).

[23] M. P. Bento, H. E. Haber, J. C. Romao, and J. P. Silva, Multi-Higgs doublet models: Physical parametrization, sum rules and unitarity bounds, J. High Energy Phys. 11 (2017) 095.

[24] Q. H. Cao, E. Ma, and G. Rajasekaran, Observing the dark scalar doublet and its impact on the standard-model Higgs boson at colliders, Phys. Rev. D **76**, 095011 (2007).

[25] E. Lundstrom, M. Gustafsson, and J. Edsjo, The inert doublet model and LEP II limits, Phys. Rev. D **79**, 035013 (2009).

[26] ATLAS Collaboration, CERN Report No. ATLAS-CONF-2020-052, 2020, https://cds.cern.ch/record/2743055.

[27] N. Aghanim *et al.* (Planck Collaboration), Planck 2018 results. VI. Cosmological parameters, Astron. Astrophys. **641**, A6 (2020).

[28] G. Belanger, F. Boudjema, A. Pukhov, and A. Semenov, micrOMEGAs_3: A program for calculating dark matter observables, Comput. Phys. Commun. **185**, 960 (2014).

[29] E. Aprile *et al.* (XENON Collaboration), Dark Matter Search Results from a One Ton-Year Exposure of XENON1T, Phys. Rev. Lett. **121**, 111302 (2018).

[30] C. Karwin, S. Murgia, T. M. P. Tait, T. A. Porter, and P. Tanedo, Dark matter interpretation of the Fermi-LAT observation toward the Galactic Center, Phys. Rev. D **95**, 103005 (2017).

[31] G. Bélanger, K. Kannike, A. Pukhov, and M. Raidal, Minimal semi-annihilating $\mathbb{Z}_N$ scalar dark matter, J. Cosmol. Astropart. Phys. 06 (2014) 021.

[32] F. Gianotti *et al.*, Physics potential and experimental challenges of the LHC luminosity upgrade, Eur. Phys. J. C **39**, 293 (2005).

[33] T. Lesiak, Future e^+e^- colliders at the energy frontier, EPJ Web Conf. **206**, 08001 (2019).